Cancer Research

TMEM16A Induces MAPK and Contributes Directly to Tumorigenesis and Cancer Progression

Umamaheswar Duvvuri[1,7], Daniel J. Shiwarski[1], Dong Xiao[1], Carol Bertrand[2], Xin Huang[6], Robert S. Edinger[5], Jason R. Rock[10], Brian D. Harfe[11], Brian J. Henson[8,9], Karl Kunzelmann[12], Rainer Schreiber[12], Raja S. Seethala[3], Ann Marie Egloff[1], Xing Chen[1], Vivian W. Lui[1], Jennifer R. Grandis[1,4], and Susanne M. Gollin[1,3,8,9]

Abstract

Frequent gene amplification of the receptor-activated calcium-dependent chloride channel TMEM16A (TAOS2 or ANO1) has been reported in several malignancies. However, its involvement in human tumorigenesis has not been previously studied. Here, we show a functional role for TMEM16A in tumor growth. We found TMEM16A overexpression in 80% of head and neck squamous cell carcinoma (SCCHN), which correlated with decreased overall survival in patients with SCCHN. TMEM16A overexpression significantly promoted anchorage-independent growth *in vitro*, and loss of TMEM16A resulted in inhibition of tumor growth both *in vitro* and *in vivo*. Mechanistically, TMEM16A-induced cancer cell proliferation and tumor growth were accompanied by an increase in extracellular signal–regulated kinase (ERK)1/2 activation and cyclin D1 induction. Pharmacologic inhibition of MEK/ERK and genetic inactivation of ERK1/2 (using siRNA and dominant-negative constructs) abrogated the growth effect of TMEM16A, indicating a role for mitogen-activated protein kinase (MAPK) activation in TMEM16A-mediated proliferation. In addition, a developmental small-molecule inhibitor of TMEM16A, T16A-inh01 (A01), abrogated tumor cell proliferation *in vitro*. Together, our findings provide a mechanistic analysis of the tumorigenic properties of TMEM16A, which represents a potentially novel therapeutic target. The development of small-molecule inhibitors against TMEM16A may be clinically relevant for treatment of human cancers, including SCCHN. *Cancer Res; 72(13); 3270–81. ©2012 AACR.*

Introduction

Amplification of the chromosomal band 11q13 is frequently seen in malignancies arising from breast, bladder, head and neck (SCCHN), and esophagus (1). Detailed molecular analysis of the 11q13 region led to identification of *TMEM16A* (also known as *TAOS2*, *DOG1*, and *ANO1*; refs. 2–4). This gene belongs to the TMEM16 family, characterized by the presence of 8 transmembrane domains and a highly conserved domain of unknown function (DUF590).

Recently, TMEM16A was shown to be a calcium-activated chloride channel (CaCC; refs. 5–7). The biologic importance of Tmem16a is underscored by the lethal phenotype in the knockout mouse because of abnormal tracheal development (8–10). TMEM16A contributes to many important physiologic functions, including the control of epithelial fluid transport, saliva production, and gastrointestinal tract motility (10–14). The third extracellular loop of TMEM16A (between transmembrane regions 5 and 6) has been suggested to be the putative pore-forming domain (6). Using mutagenesis approaches, the lysine residue at amino acid 610 (in the putative pore region) was found to be critical for its channel function (15). Specifically, mutation of this residue from lysine to alanine (TMEM16A-K610A) was shown to be hypomorphic, with greatly reduced chloride conductance.

CaCCs can be proapoptotic and suppress tumor formation in breast epithelia (16). However, there are exceptions, the putative CaCC, bestrophin (BEST1) is upregulated in colon cancer cells, and can promote proliferation (17). In addition, several reports have shown that TMEM16A is overexpressed in many tumor types including esophageal cancers, gastrointestinal stromal tumors, and SCCHN (18–20). These seemingly discordant findings prompted us to investigate the role of TMEM16A in epithelial malignancies.

We initially determined the effects of TMEM16A on tumor proliferation (*in vitro* and *in vivo*) through gain- and loss-of-function experiments. Our results show that TMEM16A

Authors' Affiliations: Departments of [1]Otolaryngology, [2]Cell Biology and Physiology, [3]Pathology, [4]Pharmacology and Chemical Biology, and [5]Renal and Electrolyte Division, University of Pittsburgh Medical Center; [6]Department of Obstetrics, Gynecology, and Reproductive Sciences, University of Pittsburgh School of Medicine and Magee-Women's Research Institute, University of Pittsburgh Medical Center; [7]Veterans Affairs Pittsburgh Health System; [8]University of Pittsburgh Cancer Institute; [9]Human Genetics, University of Pittsburgh Graduate School of Public Health, Pittsburgh, Pennsylvania; [10]Department of Cell Biology, Duke University Medical Center, Durham, North Carolina; [11]Department of Molecular Genetics and Microbiology and the Genetics Institute, University of Florida, Gainesville, Florida; and [12]Department of Physiology, University of Regensburg, Regensburg, Germany

Note: Supplementary data for this article are available at Cancer Research Online (http://cancerres.aacrjournals.org/).

Current address for J.R. Rock: Department of Anatomy, University of California San Francisco.

Corresponding Author: Umamaheswar Duvvuri, University of Pittsburgh, 200 Lothrop Street, W948 Biomedical Science Tower, Pittsburgh, PA 15213. Phone: 412-647-0954; Fax: 412-647-2080; E-mail: duvvuriu@upmc.edu

doi: 10.1158/0008-5472.CAN-12-0475-T

induces potent and specific stimulation of the extracellular signal–regulated kinase (ERK)1/2 (as determined by phospho-ERK1/2), and contributes to the growth of cancer cell lines. These studies provide, to the best of our knowledge, the first mechanistic description of the role of TMEM16A in human malignancies and suggest that this protein may play an important role in facilitating tumor growth.

Materials and Methods

TMEM16A antibody and immunoblotting

A rabbit polyclonal serum was obtained by immunizing rabbits with an epitope (CARVLEKSLKKESRNKEKR) from exon 14 of TMEM16A. This epitope was chosen on the basis of a BLAST search that defined a unique 21 amino-acid sequence. For immunoblotting, equal amounts of protein were separated on SDS-PAGE and transferred to nitrocellulose membranes. The membranes were then probed with anti-TMEM16A serum, phospho-ERK1/2, pERK1/2, p-ERK5, ERK5, B-Raf, C-Raf, phospho-AKT Ser 472, AKT (Cell Signaling), and Cyclin D1 M-20 (Santa Cruz). β-Tubulin or actin was used as a loading control. Ras activation kit was used according to instructions (Millipore, EMD). All immunoblots were scanned at 600 dpi and postprocessed using Photoshop software (Adobe Systems). Any manipulation was applied to the entire image to preserve image integrity.

Cell culture

HEK-293T cells were obtained from American Type Culture Collection (ATCC; Manassas, VA). UM-SCC1 and T24 cells were obtained from the University of Michigan (a gift from Dr Thomas Carey). EPC1 cells were a gift from Dr H. Nakagawa. All cell lines were genotyped to establish identity within 6 months of experimentation. Stable overexpressing clones were made using DNA transfection or retroviral infection. Cells were selected after transduction and viable cells were pooled. Individual clones were identified by the method of limiting dilutions. Each clone was kept for 10 passages, after which an early passage sample was thawed and used.

Plasmid/siRNA transfections, retrovirus generation, shRNA transduction

Plasmid transfections were conducted using Fugene (DNA) or Lipofectamine 2000 (siRNA) according to the manufacturer's instructions. *TMEM16A* and *TMEM16A-K610A* mutant were subcloned into pBabe-puro vectors. Retroviruses were generated by transfecting PhoenixAmpho cells with these plasmids. Lentiviral shRNA and retroviral particles were used to transduce cells. Antibiotic selection was carried out. All transduction experiments were repeated at least 3 separate times to ensure reproducibility. GFP-tagged dominant negative ERK2 construct was previously described (21). *ERK1/2* siRNA was obtained from Cell Signaling.

Whole-cell patch clamping

Whole-cell patch clamping was conducted as previously described (22). All pipette solutions were previously described (22). All experiments used a standard protocol that alternated a current–voltage (I/V) step measurement. The I/V measurement stepped the holding potential from −100 to +100 mV in 20 mV steps. All patch clamp results were normalized by the cell capacitance recorded at the start of the experiment.

MQAE fluorescence assays

MQAE chloride efflux assays were conducted on cells plated onto optical Petri dishes (Matek) precoated with poly-L-lysine as previously described (23). MQAE was introduced into the cells using a hypotonic shock followed by recovery for 10 minutes before the start of the experiment. The MQAE-loaded cells were then mounted on the stage of an IX-81 Olympus microscope and perfused to 37°C. MQAE fluorescence intensity was captured every 15 seconds at the 445-nm wavelength in response to excitation at 340 nm.

The magnitude of fluorescence in each cell in the field was quantified from a circular region of interest (ROI) drawn within the cell, and the time course of fluorescence change was plotted as the average ± SEM of all ROIs in the field (typically 10–50 cells, "n") for a single coverslip. The rate of change in fluorescence upon the switch from high chloride to low chloride was determined for each ROI. All ROIs exhibiting a positive, linear rate of change ($R^2 \geq 0.75$) from at least 3 separate, identical experiments (coverslips, "N") were pooled, and statistical significance was assessed for all ROIs using Student's t test.

Cell viability assay and drug treatments

For proliferation and viability analysis, cells were plated in 96-well optical plates at 5×10^3 cells/well. The plates were treated the following day, as indicated. One to 3 days after treatment, the CellTiter-Glo Assay (Promega) was used according to the manufacturer's directions.

Soft agar assay, anchorage-independent viability

Soft agar assays were conducted as previously described (24). Briefly, 5×10^4 cells suspended in 0.7% agar solution were plated in a 35-mm dish on top of 1.4% agar. Colonies were counted 3 weeks after plating. Colonies with a diameter greater than 100 μm were counted using crystal violet. Anchorage-independent viability was determined by plating cells (5×10^3) in poly-HEMA coated plates as previously described (25). Cell viability was assessed 3 days after plating.

In vivo growth

All animal studies were conducted under approval from the University of Pittsburgh and were conducted in accordance with established guidelines. Nude mice were injected on each flank and subsequent tumor volumes were measured when a palpable tumor was noticed. Measurements of length and width were recorded and used to determine the volume of each tumor. At the conclusion of the experiment, tumors were harvested and processed for further evaluation.

Primary tissue samples, tissue array

Paired normal and tumor tissues were collected after obtaining informed consent and approval from our Institutional Review Board. Normal adjacent mucosa is defined as histologically benign appearing mucosa (as judged by an experienced pathologist) acquired from the margins of the tumor

resection. Tissue arrays containing replicate cores were created from patients who underwent curative surgery for SCCHN at our institution. Staining was conducted with anti-TMEM16A antisera and scored using a semiquantitative system (H-score) and the results correlated with survival. H-score was defined as the relative intensity, scored on a 0 to 3 scale, multiplied by the percentage of positively stained cells. The H-scores for the population were analyzed to determine the median score. High and low expressors were categorized as having H-scores above or below the median.

Oncomine analysis

Data were abstracted from the Oncomine database, and used to assess the relative expression of TMEM16A in tumors versus normal adjacent mucosa. We specifically evaluated the expression the RefSeq version of TMEM16A: NM_018043.5. A fold-change of at least 3 was used as a cut-off value.

FISH studies

FISH studies were carried out on the tissue microarray using a probe for the centromere of chromosome 11 (CEP11) labeled with SpectrumGreen (Abbott Molecular) and a probe prepared from a BAC clone (RP11-805J14; CHRI) and labeled by nick translation with SpectrumOrange. Slide processing and scoring were described previously (26).

Knockout mouse experiments

Tmem16a knockout mice were generated as previously described (8, 9). Tissues were obtained by dissecting the oral cavity mucosa from mice after genotyping. Tissues were snap frozen and subsequently used for immunochemistry, RT-PCR, and immunoblotting as described earlier.

Quantitative reverse transcription-PCR

The reverse transcriptions were carried out with predesigned TaqMan primer and probe pairs as described earlier (2). Reverse transcriptase (RT) controls were carried out for each RNA input each time. Quantitative PCR (qPCR) was conducted for *TMEM16A* and *GAPDH* was used as an endogenous control. The primer and probe sequences, conditions, and concentration have been described previously (4).

Statistical analysis

All data are reported as mean ± SEM unless stated otherwise. Cell viability and tumor xenograft measurements were analyzed with a 2-tailed Student's t test. A paired t test was used to test for differences in TMEM16A expression between matched tumor and benign mucosa. A two-sided Mann–Whitney rank-sum test was used to test the association of overexpression of TMEM16A with 11q13 amplification and TMEM16A expression on IHC. Kaplan–Meier and log rank tests of equality of survivors were used to evaluate differences in overall survival or disease-specific survival by high versus low TMEM16A IHC scores, as defined by the median value. Multivariable Cox proportional hazards models were used to evaluate TMEM16A tumor protein levels as a predictor of overall survival after adjusting for age, sex, and disease stage. The assumption of proportional hazards was tested by evaluation of Schoenfeld residuals. $P < 0.05$ was considered as statistically significant.

Results

TMEM16A overexpression correlates with decreased survival in SCCHN

To examine the protein expression profile, rabbit polyclonal antibody to TMEM16A, was generated and used for immunoblotting and IHC (Supplementary Fig. S1a and S1b). As expected, Tmem16a derived from murine tissues migrates at a higher molecular weight (~150 kDa) than human TMEM16A (~115 kDa). This is consistent with previously published data (6). We further validated this antibody's specificity in IHC by evaluating tissues obtained from wild-type and knockout mice.

TMEM16A protein is overexpressed by 5-fold in tumors when compared with paired adjacent normal mucosa (Fig. 1A and B; $P < 0.001$). Overexpression was noted in 14/17 (83%) samples. Next, we confirmed that TMEM16A mRNA is overexpressed by 5-fold in a separate cohort of primary tumors and paired adjacent normal mucosa (Fig. 1C; $P < 0.05$).

TMEM16A is endogenously expressed in benign secretory tissues such as salivary gland and breast tissue (14). We therefore wanted to confirm that breast malignancies also overexpress TMEM16A. We used the Oncomine database to determine the expression of *TMEM16A* in normal and malignant tissues from a variety of tumor types. We found that although *TMEM16A* may be expressed at a high level in normal breast tissue, its expression is even higher in neoplastic breast tissue (Fig. 1D). This suggests that although endogenous *TMEM16A* expression may be high in some normal tissues, malignant cells derived from these tissues further upregulate *TMEM16A*. This finding implicates *TMEM16A* as a potential target gene in malignant transformation.

We then determined the association between TMEM16A overexpression and clinical outcome of patients with SCCHN. TMEM16A expression was detected in approximately 85% of SCCHN tumors. Kaplan–Meier survival analysis showed that patients with high-level tumor expression of TMEM16A had decreased overall survival ($P = 0.04$, log rank test; Fig. 1E). High TMEM16A tumor levels tended to be associated with decreased overall survival in a univariable Cox proportional hazards model (HR = 3.04; 95% CI, 0.97–9.46) and in a multivariable Cox proportional hazards model adjusting for age, sex, and nodal stage (HR = 2.8; 95% CI, 0.86–9.16).

However, Kaplan–Meier analysis showed no significant correlation between overall or disease-free survival and *TMEM16A* gene amplification (Supplementary Fig. S2a and S2b). Although patients whose tumors harbored *TMEM16A* amplification had a median survival of 50.7 months, whereas those not amplified for *TMEM16A* did not reach a median survival, suggesting that there may be a trend toward improved survival in patients without gene amplification. Gene amplification was not strongly correlated with protein expression.

TMEM16A promotes tumor growth and proliferation

Next, we investigated the effects of *TMEM16A* manipulation (through gain-of-function and loss-of-function) on the

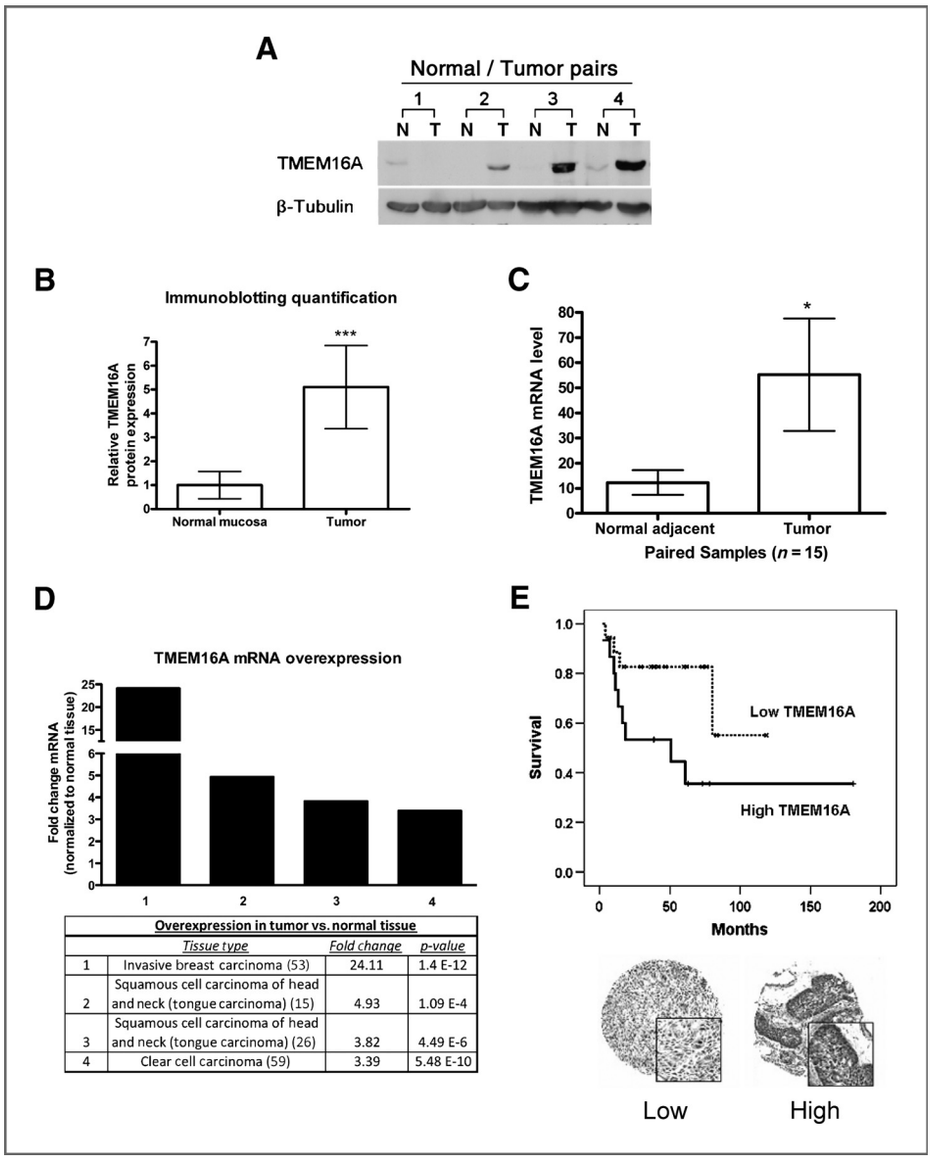

Overexpression in tumor vs. normal tissue			
	Tissue type	*Fold change*	*p-value*
1	Invasive breast carcinoma (53)	24.11	1.4 E-12
2	Squamous cell carcinoma of head and neck (tongue carcinoma) (15)	4.93	1.09 E-4
3	Squamous cell carcinoma of head and neck (tongue carcinoma) (26)	3.82	4.49 E-6
4	Clear cell carcinoma (59)	3.39	5.48 E-10

Figure 1. TMEM16A is overexpressed in SCCHN and correlates with decreased survival. TMEM16A expression is upregulated in 17 paired tumor (T) versus paired adjacent normal mucosa (N) as detected by immunoblotting (A). There is a 5-fold increase of TMEM16A expression in tumors relative to normal adjacent mucosa (B; mean ± SEM; $n = 17$; ***, $P < 0.001$). A 5-fold increase in tumor: normal TMEM16A mRNA was observed in a separate cohort (C; $n = 15$; *, $P < 0.05$). TMEM16A expression data were abstracted from Oncomine and analyzed for relative overexpression (D). High TMEM16A expression was associated with decreased overall patient survival (E; $n = 34$, $P < 0.05$). Representative images of TMEM16A staining are shown.

proliferation of cancer cells (Supplementary Fig. S3a and S3b). To evaluate the role of *TMEM16A* independently of 11q13 amplification, we chose to use the UM-SCC1 SCCHN cell line (that harbors 11q13 amplification) and the T24 bladder cancer cell line (that does not contain the 11q13 amplicon). Lentiviral shRNA was used to "knock-down" *TMEM16A* in both cell lines. We identified 2 independent shRNA sequences that caused a significant reduction (~80%) in TMEM16A protein expression. TMEM16A knockdown led to a measurable change in whole-cell chloride conductance (~50%), as assayed by MQAE fluorescence assays (Supplementary Fig. S3c–S3e; ref. 27). Forced overexpression of a mutant version of *TMEM16A* (*TMEM16A*-K610A) led to significantly smaller chloride conductance (Supplementary Fig. S3f). For further experiments, we used one of the sequences (shRNA#5).

To determine the consequences of *TMEM16A* knockdown on *in vivo* tumor growth, shRNA-treated UM-SCC1 cells were inoculated subcutaneously into nude mice. *TMEM16A* shRNA led to a significant decrease in xenograft growth (Fig. 2A and B). Furthermore, we found that TMEM16A shRNA-treated tumors exhibited decreased Ki-67 staining (Fig. 2C and D). Several reports have showed that the mitogen-activated protein kinase (MAPK)/ERK signaling pathway enhances the growth of epithelial cancer cells, in particular, bladder cancer, and SCCHN (28). We noted that pERK staining was less prominent in tumors derived from *TMEM16A* shRNA-treated cells versus control shRNA tumors (Fig. 2D).

Next, we exogenously overexpressed TMEM16A in several cell lines that do not harbor endogenous gene amplification. In T24 cells, TMEM16A was trafficked to the cell surface (Supplementary Fig. S1b), led to increased chloride fluxes, and resulted in enhanced xenograft growth (Fig. 3A–C). Tumor xenografts confirmed overexpression of TMEM16A and showed increased pERK1/2 and Ki-67 staining (Fig. 3D).

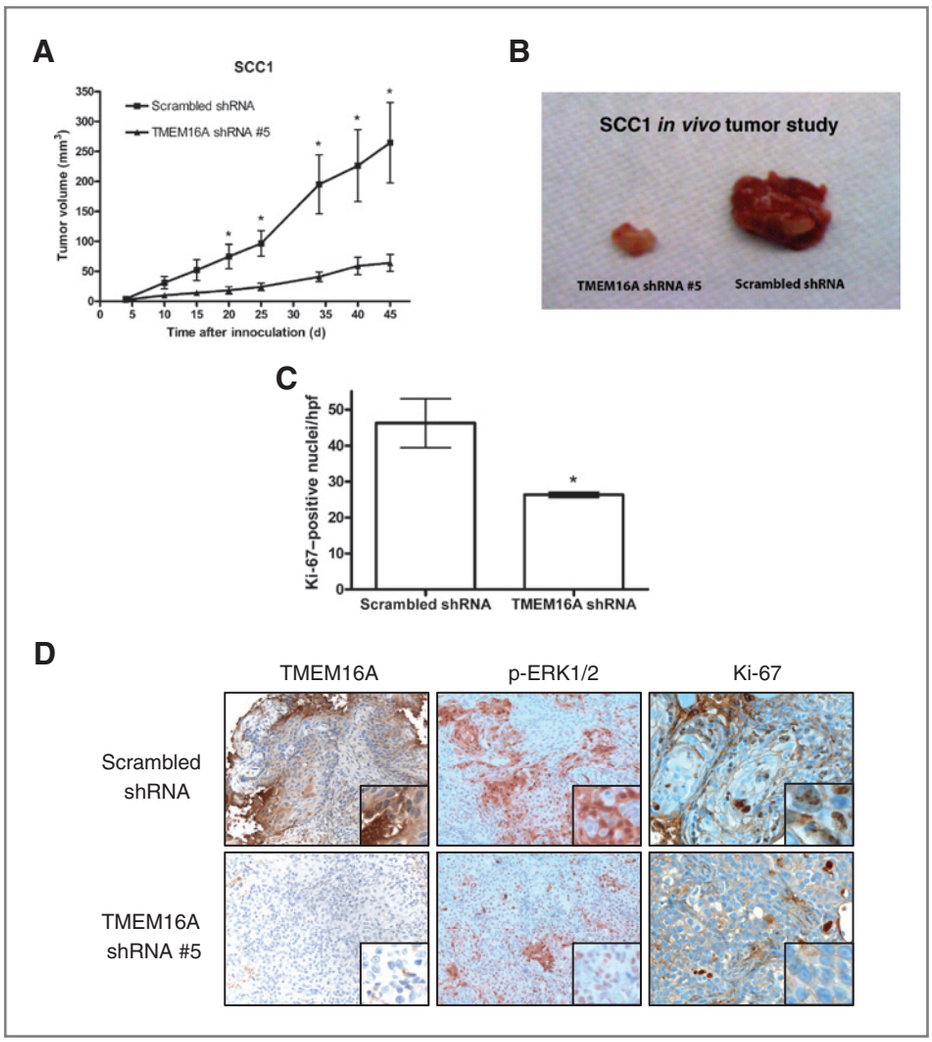

Figure 2. *TMEM16A* knockdown results in significant growth inhibition of SCCHN tumor xenografts *in vivo*. *TMEM16A* knockdown *in vivo* led to smaller tumors (A and B; *, $P < 0.05$). Xenografts generated from *TMEM16A* shRNA cells showed decreased proliferation (as determined by Ki-67 staining) and reduced pERK1/2 (C and D; *, $P < 0.05$). Representative images showing TMEM16A, pERK1/2, and Ki-67 staining are shown ($n = 6$). Inset image shows ×10 magnification. hpf, high-power field.

TMEM16A overexpression led to increased *in vitro* proliferation of HEK-293T cells, and increased anchorage-independent viability in immortalized keratinocytes (Supplementary Fig. S4a and S4b). TMEM16A knockdown in 2 other cell lines (Cal33 and PCI-15B) suppressed cell growth *in vitro* (Supplementary Fig. S4c). Furthermore, TMEM16A cooperated with constitutively active H-RAS to induce focus formation in immortalized MEFs (Supplementary Fig. S4d). Similarly, forced overexpression of TMEM16A conferred increased colonogenic survival in immortalized keratinocytes and tumor cell lines (Supplementary Fig. S4e). Taken together, these data suggest that TMEM16A overexpression can facilitate oncogenic transformation through cooperation with potent oncogenes.

We next determined the effect of *TMEM16A* knockdown on *in vitro* growth. Treatment with *TMEM16A* shRNA led to a significant retardation in proliferation when compared with control shRNA (Fig. 4A and B). *TMEM16A* shRNA abrogated the increase in both anchorage-dependent and -independent cell proliferation noted in overexpressing cells (Fig. 4C and D). *TMEM16A* knockdown induced an accumulation of cells in G_0/G_1 and a concomitant decrease in the S/G_2 phase, suggesting a block in cell-cycle progression (Supplementary Fig. S5a). Interestingly, TMEM16A overexpression impaired caspase-3/7 activation, suggesting that TMEM16A may in fact impair apoptotic cell death, along with promoting cell growth (Supplementary Fig. S5b).

TMEM16A induces phosphorylation of ERK1/2

Because we observed differential expression of pERK1/2 in tumor xenografts, we examined whether *TMEM16A* expression influenced ERK1/2 activation. *TMEM16A* overexpression was associated with an increase in phosphorylated ERK1/2 (~2-fold) and cyclin D1 (~5-fold; Fig. 5A). *TMEM16A* siRNA led to a decrease in phospho-ERK1/2 and cyclin D1 (Fig. 5B). We noted that AKT and phospho-AKT levels were not significantly influenced by *TMEM16A* overexpression, suggesting specificity to the ERK1/2 pathway (Fig. 5B). Similarly, there were no changes in p-ERK5 or ERK5 (Supplementary Fig. S6c).

It is well known that RAS oncogenic signaling can activate ERK1/2. *HRAS*, in particular, has been associated with SCCHN development (29, 30). In fact, no mutations in *KRAS* or *NRAS* were observed in 2 recent genomic studies of

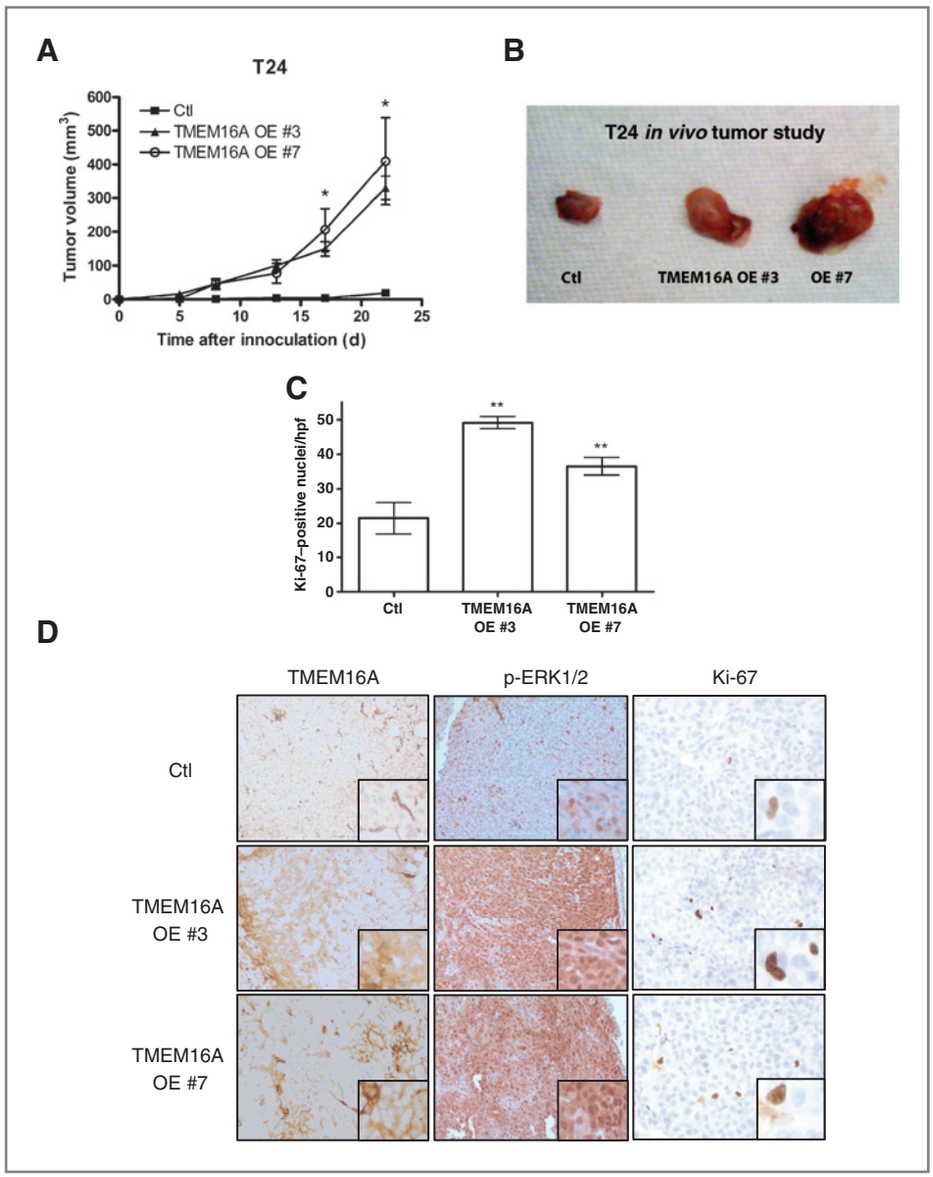

Figure 3. *TMEM16A* overexpression (OE) induces *in vivo* tumor growth. Overexpression of TMEM16A markedly promoted tumor growth in the T24 xenograft model (A and B). TMEM16A-overexpressing cells showed increased proliferation (as determined by Ki-67 staining) and pMAPK staining (C and D; **, $P < 0.01$). Increased levels of p-ERK1/2 are also found in tissue derived from tumor explants (D). Inset image shows ×10 magnification. OE3 and OE7 refer to individual clones. Ctl, control; hpf, high-power field.

SCCHN (30, 31). We therefore evaluated the presence of *HRAS, KRAS*, and *NRAS* mutations in the cell lines used in this study. T24 cells harbor the activating *HRAS*G12V mutation, however, HEK-293T, EPC1, and UM-SCC1 cells did not harbor mutant *HRAS*, *KRAS*, or *NRAS* (data not shown). Taken together, these data suggest that the impact of TMEM16A on ERK1/2 signaling is independent of activating *HRAS* mutations.

Next, we explored the association between *Tmem16a* and *cyclinD1* in oral cavity tissues obtained from wild-type and Tmem16a$^{-/-}$ embryos. As expected, Tmem16a levels were reduced in knockout mouse tissues as compared with wild-type and heterozygous mice (Fig. 5C). Interestingly, cyclin D1 was also decreased in tissues derived from knockout mice, but not in their heterozygous or wild-type littermates. We observed intense nuclear cyclin D1 staining in the proliferative mesoderm of wild-type mice but not in the *Tmem16a*$^{-/-}$ littermates (Supplementary Fig. S6a). We further explored this finding by measuring mRNA expression of *Tmem16a* and *Ccnd1* in these tissues. As expected, knockout tissues had significantly lower levels of cyclin D1 (Supplementary Fig. S6b). This finding suggested that TMEM16A may be influencing cell proliferation on a fundamental level and occurs *in vivo*.

We postulated that if TMEM16A affects proliferation by activating MEK/ERK, inhibition of MEK/ERK should abrogate *TMEM16A*-induced growth. Indeed, treatment with either UO126 or dominant-negative ERK1/2 led to a complete abrogation of *TMEM16A*-induced growth (Fig. 5D and E). Similar data were observed with the specific ERK inhibitor AZD6244 and with siRNA against ERK1/2 (Supplementary Fig. S5c and S5d). Treatment with TMEM16A shRNA

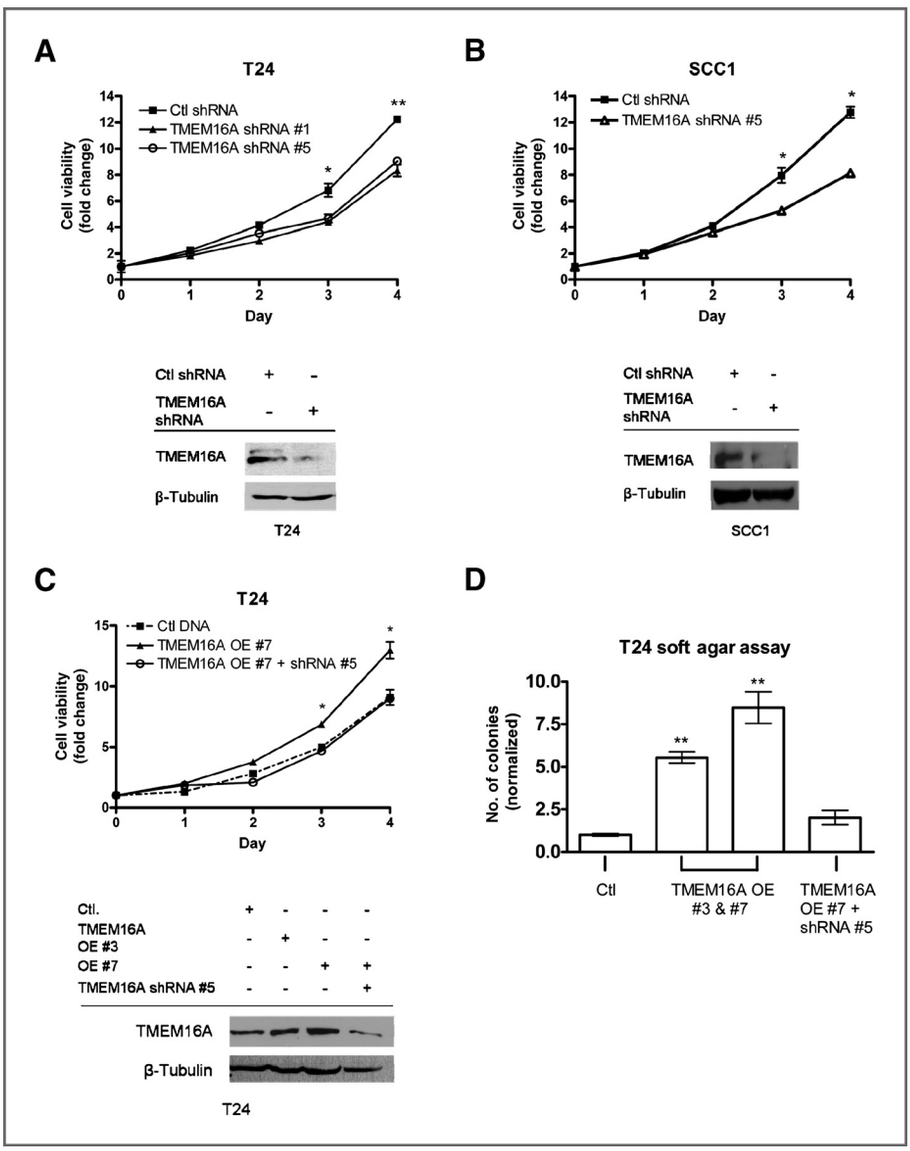

Figure 4. TMEM16A expression mediates both anchorage-dependent and -independent growth. TMEM16A knockdown caused a decrease in proliferation (mean ± SEM; $n = 3$; *, $P < 0.05$; A and B). Representative immunoblots are shown. The growth advantage conferred by TMEM16A overexpression was abrogated by shRNA (C; mean ± SEM; $n = 3$, $P < 0.05$). Immunoblotting confirms overexpression (OE) and subsequent knockdown of TMEM16A (C). Soft agar colony formation was also enhanced by TMEM16A overexpression and rescued by subsequent knockdown (D; mean ± SEM; $n = 4$, $P < 0.01$).

reversed the activation of MEK and ERK1/2 induced by TMEM16A overexpression (Fig. 5F). This observation suggests that TMEM16A overexpression directly impacts ERK1/2 activation.

Recent data suggests that ERK activation may impact the chloride conductance of TMEM16A (15). Similarly, mutations in the putative pore forming domain can impact the whole-cell chloride conductance in forced overexpression experiments (32). We sought to determine if the putative pore-forming region of *TMEM16A* was necessary for activation of ERK1/2. Forced overexpression of a mutant version of *TMEM16A* (*TMEM16A*-K610A) that has been described to display significantly abrogated chloride conductance (15) did not induce ERK1/2 or phospho-ERK1/2 (Fig. 6A). We verified that TMEM16A-K610A was trafficked to the cell membrane using biotinylation experiments (data not shown). Our data raise the intriguing possibility that TMEM16A affects ERK activation by modulating intracellular chloride levels. Unfortunately, manipulation of intracellular chloride levels can itself induce changes in the expression of ion channels. Therefore, further work is necessary to dissect the effect of intracellular chloride on ERK activation.

Overexpression of mutant *TMEM16A-K610A* did not promote anchorage-independent viability compared with vector controls (Fig. 6B–D). To confirm that the effects are indeed directly dependent on *TMEM16A* expression, we rescued *TMEM16A* shRNA-treated cells with shRNA-resistant versions of *TMEM16A* or *TMEM16A-K610A* (Supplementary Fig. S7a). The reduction in viability induced by *TMEM16A* shRNA was rescued by expression of an shRNA-resistant version of *TMEM16A*, but not resistant *TMEM16A-K610A* (Fig. 6E). This approach provides strong evidence to show that TMEM16A directly induces the proliferative phenotype.

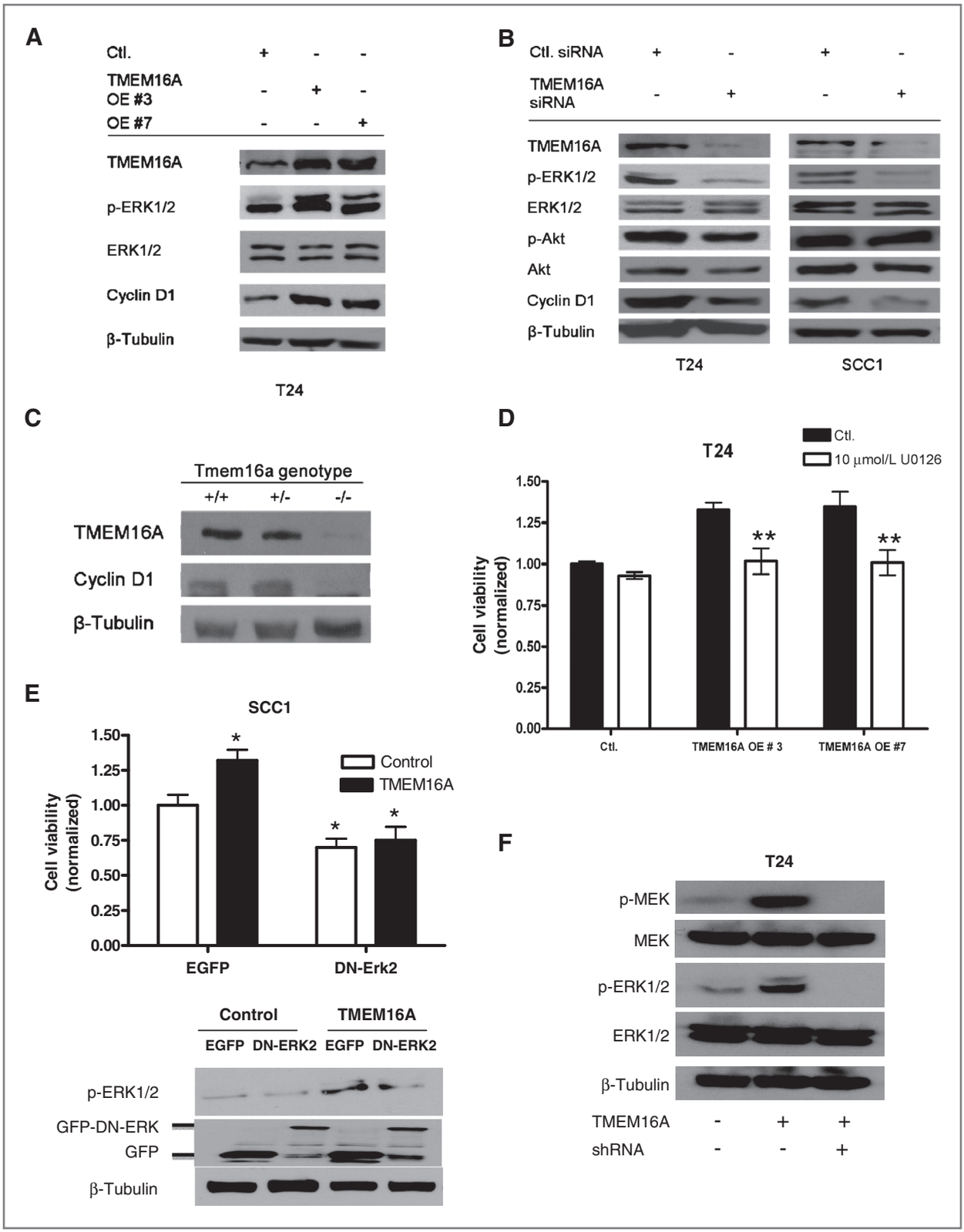

Figure 5. The mitogenic phenotype of TMEM16A is associated with ERK1/2 activation. TMEM16A overexpression induced phospho-ERK1/2 and cyclin D1 (A). TMEM16A-siRNA led to decreased phospho-ERK1/2 and cyclin D1. Phospho-Akt levels were not consistently modulated by TMEM16A manipulation (B). The relationship between TMEM16A and cyclin D1 in head and neck tissues derived from Tmem16a knockout (−/−) versus wild-type (+/+) or heterozygous (+/−) mice (C). ERK inhibition with UO126 or dominant-negative ERK2 abrogated the growth advantage in overexpressing cells (D and E; mean ± SEM; $n = 3$; **, $P < 0.01$). Treatment of overexpressing cells with *TMEM16A* shRNA abrogated the activation MEK and ERK1/2 (F). Ctl, control.

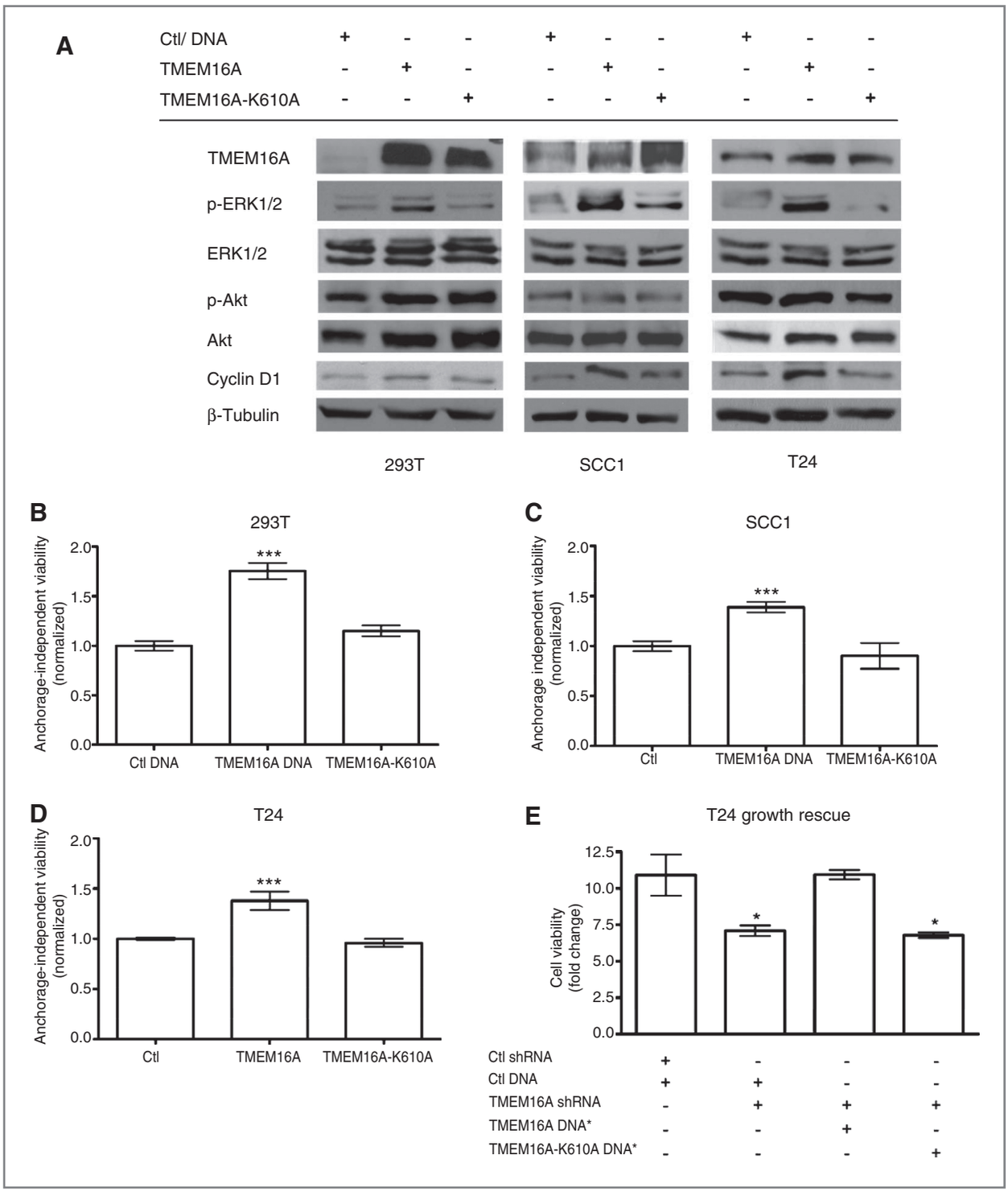

Figure 6. The putative pore-forming region of TMEM16A mediates ERK1/2 activation and subsequent mitogenic effects. Expression of the *TMEM16A-K610A* mutant fails to induce ERK1/2 and cyclin D1 (A). TMEM16A-K610A did not increase anchorage-independent viability (B–D; mean ± SEM; $n = 3$; ***, $P < 0.001$). TMEM16A shRNA–induced decrease in growth was subsequently rescued with TMEM16A shRNA–resistant DNA (*TMEM16A* DNA*), but not with *TMEM16A-K610A* shRNA–resistant DNA (*TMEM16A-K610A* DNA*; E; mean ± SEM; $n = 3$, $P < 0.05$). Ctl, control.

TMEM16A activates the Ras-Raf-MEK-ERK pathway

The observation that TMEM16A induces activation of ERK1/2 led us to interrogate the RAS-RAF-MEK-ERK1/2 pathway. Indeed we observed robust activation of RAS-RAF-MEK-ERK pathway upon TMEM16A overexpression (Fig. 7A and B). Densitometric quantitation is shown in Supplementary Fig. S7b. Interestingly, this activation was independent of *HRAS* mutation status, because T24 cells harbor an activating *HRAS* mutation, but SCC1 cells do not (data not shown). We next sought to determine if Ras inhibition (using a dominant negative construct) could abrogate the observed phenotype. Forced overexpression of a dominant-negative mutant of H-Ras (H-RasN17) abrogated the observed activation of MEK, ERK1/2 and also the growth phenotype (Fig. 7C and D).

Pharmacologic inhibition of TMEM16A induces cancer cell death

To validate TMEM16A as a potential target in epithelial malignancies, we wanted to determine if small-molecule inhibition of TMEM16A could inhibit tumor cell proliferation. Therefore, we treated UM-SCC1 and T24 cells with a novel TMEM16A inhibitor (T16A-inh01; refs. 33, 34). T16A-inh01 induced a dose-dependent reduction in cell viability (Supplementary Fig. S8a and S8B). To determine whether combined inhibition of *TMEM16A* and MAPK had an additive effect on cell viability, we treated cells with the MEK/ERK inhibitor UO126 alone or in combination with TMEM16A shRNA. TMEM16A knockdown resulted in a modest decrease in cell proliferation, however, we observed an additive effect with MAPK inhibition (Supplementary Fig. S8c and S8d). The chemical structure of T16A-inh01 is shown in Supplementary Fig. S8e. We did not observe additive inhibitory effects on ERK phosphorylation. These data show that TMEM16A and MAPK inhibition may act in an additive fashion to retard tumor cell proliferation, suggesting that ERK1/2 may not uniquely control TMEM16A-induced cell growth.

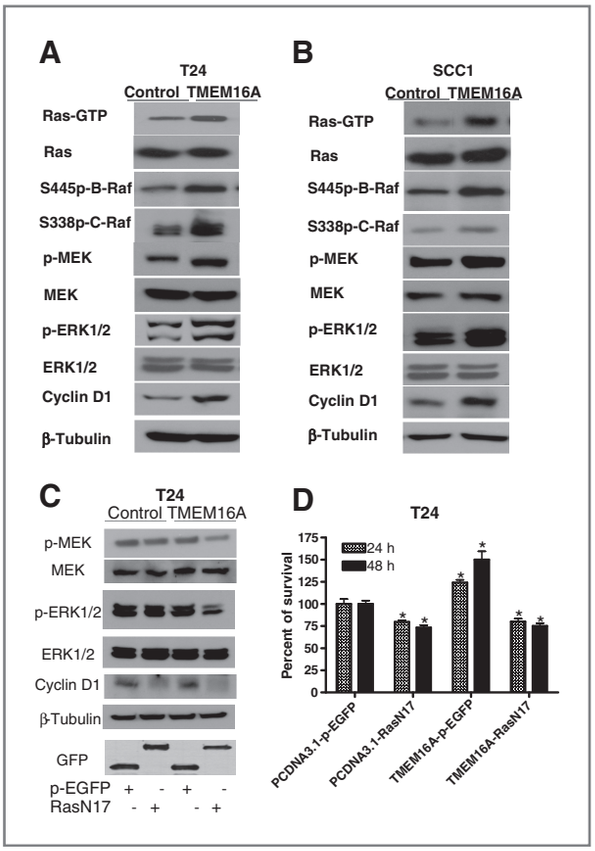

Figure 7. TMEM16A expression activates the Ras-Raf-MEK-ERK1/2 pathway. Activation of Ras, B-Raf, and C-Raf was observed in T24 and UM-SCC1 cells after TMEM16A overexpression (A and B). Activation of the pathway was abrogated by forced expression of dominant-negative Ras (C). Forced expression of dominant-negative Ras abrogated the growth advantage conferred by TMEM16A overexpression (D).

Discussion

There is accumulating evidence that chloride channels influence tumor growth and progression (35–37), however the mechanism(s) by which this occurs remains unclear. Calcium-activated chloride channels (CaCCs) are a unique subset of chloride channels that play important roles in many fundamental physiologic processes (38, 39). Recently, ANO1/TMEM16A was described as a *bona fide* CaCC (5–7). However, it remains controversial whether TMEM16A is itself a functional CaCC, or forms a subunit within the protein complex that facilitates CaCC activity (7, 40, 41). Recent reports suggest that CaCCs can both promote and retard tumor cell proliferation (16, 17). These contradictory reports suggest that improved understanding of the impact of CaCC regulation and activation on cell proliferation may help to define whether these molecules can serve as a future therapeutic target.

TMEM16A is frequently overexpressed in several tumors including squamous cell carcinoma of the head and neck, esophageal cancer, and gastrointestinal stromal tumors (GIST; refs. 4, 18, 42, 43). To date, the exact role(s) that TMEM16A plays in tumor development/progression remains unclear. Ayoub and colleagues have recently reported that TMEM16A overexpression facilitates cell motility and may contribute to the development of metastases (44); however, no mechanism was proposed to explain this phenotype.

This report provides the first mechanistic link between TMEM16A expression and cell proliferation in human cancer. Our data show that TMEM16A expression directly impacts cellular proliferation. TMEM16A also cooperates with oncogenic H-RAS to induce focus formation in immortalized MEFs. Taken together, these data strongly suggest that TMEM16A may function as a proto-oncogene, and that its overexpression drive tumor growth.

It has recently been shown that TMEM16A channel activity is linked to ERK1/2 activation and that the ERK inhibitor UO126 can inhibit TMEM16A channel function (15). Our data suggest that TMEM16A activates the RAS-RAF-MEK-ERK1/2 pathway, thereby influencing cellular proliferation. However, this activation does not occur when a hypomorphic mutant

(TMEM16A-K610A) is expressed. These data raise the intriguing possibility that the chloride conductance of TMEM16A impacts ERK1/2 activation. However, the exact mechanism by which this occurs remains unclear.

The availability of small-molecule inhibitors against TMEM16A provides a novel potential method to inhibit tumor cell growth. The currently available small-molecule inhibitors of TMEM16A (niflumic acid and NPPB) exhibit off-target effects and have been shown to block other chloride channels. However, T16A-inh01 is a novel and potentially more specific TMEM16A inhibitor, and provides a method to inhibit channel activity (33, 34, 45). This developmental molecule likely has off-target effects, and therefore definitive conclusions cannot be defined at this time.

The ubiquitous expression of TMEM16A suggests that the endogenous protein has important physiologic roles that may be adversely impacted by pharmacologic inhibition. However, TMEM16A is known to undergo alternative splicing, and specific variants have been isolated from diseased tissues (such as diabetic gastroparesis; ref. 46–48). Recently, mutations in TMEM16A have been described in SCCHN. The existence of specific mutations in TMEM16A that have been identified from whole-exome sequencing of SCCHN, suggests that tumor-specific targeting may be possible in the future (30).

In conclusion, we have shown that TMEM16A expression: (1) is associated with decreased patient survival; (2) modulates proliferation *in vitro* and *in vivo* and induces ERK1/2 activation; (3) the pore-forming region of this molecule is necessary to facilitate these phenomena; and (4) pharmacologic inhibition (using a novel TMEM16A inhibitor) or siRNA-mediated knockdown of *TMEM16A* leads to a significant decrease in tumor cell viability by downregulating the TMEM16A-ERK1/2 signaling. In closing, these findings may describe a novel therapeutic role for TMEM16A in cancer treatment, because TMEM16A may act as a potential pharmacologic target.

Disclosure of Potential Conflicts of Interest

No potential conflicts of interest were disclosed.

Authors' Contributions

Conception and design: U. Duvvuri, D.J. Shiwarski, V.W. Lui, S.M. Gollin
Development of methodology: U. Duvvuri, D.J. Shiwarski, D. Xiao, X. Huang
Acquisition of data (provided animals, acquired and managed patients, provided facilities, etc.): U. Duvvuri, D.J. Shiwarski, D. Xiao, C. Bertrand, R.S. Edinger, J.R. Rock, R.D. Harfe, B.J. Henson, R.S. Seethala, A.M. Egloff
Analysis and interpretation of data (e.g., statistical analysis, biostatistics, computational analysis): U. Duvvuri, D.J. Shiwarski, D. Xiao, C. Bertrand, R.S. Edinger, R.S. Seethala, A.M. Egloff, X. Chen, J.R. Grandis
Writing, review, and/or revision of the manuscript: U. Duvvuri, D.J. Shiwarski, C. Bertrand, X. Huang, K. Kunzelmann, X. Chen, V.W. Lui, J.R. Grandis, S.M. Gollin
Administrative, technical, or material support (i.e., reporting or organizing data, constructing databases): U. Duvvuri, K. Kunzelmann, R. Schreiber, R.S. Seethala, X. Chen
Study supervision: U. Duvvuri, S.M. Gollin

Acknowledgments

The authors thank Dr. R.W. Sobol and the University of Pittsburgh Cancer Institute Lentiviral Facility for the generation of lentiviral particles.

Grant Support

This work was supported by the Head and Neck Cancer SPORE grant (NIH P50CA097190 J.R. Grandis), through a Veterans Administration CDA; CPPF (U. Duvvuri) and start-up funds from the Department of Otolaryngology (U. Duvvuri). The molecular cytogenetic studies were carried out in the University of Pittsburgh Cancer Institute Cytogenetics Facility, supported in part by P30CA047904 to N.E. Davidson/R.B. Herberman/S.M. Gollin. KK was supported by Deutsche Krebshilfe Projekt 109438.

The costs of publication of this article were defrayed in part by the payment of page charges. This article must therefore be hereby marked *advertisement* in accordance with 18 U.S.C. Section 1734 solely to indicate this fact.

Received February 8, 2012; revised April 26, 2012; accepted April 28, 2012; published OnlineFirst May 7, 2012.

References

1. Akervall JA, Jin Y, Wennerberg JP, Zatterstrom UK, Kjellen E, Mertens F, et al. Chromosomal abnormalities involving 11q13 are associated with poor prognosis in patients with squamous cell carcinoma of the head and neck. Cancer 1995;76:853–9.
2. Huang X, Gollin SM, Raja S, Godfrey TE. High-resolution mapping of the 11q13 amplicon and identification of a gene, TAOS1, that is amplified and overexpressed in oral cancer cells. Proc Natl Acad Sci USA 2002;99:11369–74.
3. Katoh M, Katoh M. FLJ10261 gene, located within the CCND1-EMS1 locus on human chromosome 11q13, encodes the eight-transmembrane protein homologous to C12orf3, C11orf25 and FLJ34272 gene products. Int J Oncol 2003;22:1375–81.
4. Huang X, Godfrey TE, Gooding WE, McCarty KS Jr, Gollin SM. Comprehensive genome and transcriptome analysis of the 11q13 amplicon in human oral cancer and synteny to the 7F5 amplicon in murine oral carcinoma. Genes Chromosomes Cancer 2006;45:1058–69.
5. Caputo A, Caci E, Ferrera L, Pedemonte N, Barsanti C, Sondo E, et al. TMEM16A, a membrane protein associated with calcium-dependent chloride channel activity. Science 2008;322:590–4.
6. Yang YD, Cho H, Koo JY, Tak MH, Cho Y, Shim WS, et al. TMEM16A confers receptor-activated calcium-dependent chloride conductance. Nature 2008;455:1210–5.
7. Schroeder BC, Cheng T, Jan YN, Jan LY. Expression cloning of TMEM16A as a calcium-activated chloride channel subunit. Cell 2008;134:1019–29.
8. Rock JR, Futtner CR, Harfe BD. The transmembrane protein TMEM16A is required for normal development of the murine trachea. Dev Biol 2008;321:141–9.
9. Rock JR, Harfe BD. Expression of TMEM16 paralogs during murine embryogenesis. Dev Dyn 2008;237:2566–74.
10. Rock JR, O'Neal WK, Gabriel SE, Randell SH, Harfe BD, Boucher RC, et al. Transmembrane protein 16A (TMEM16A) is a Ca^{2+}-regulated Cl^- secretory channel in mouse airways. J Biol Chem 2009;284:14875–80.
11. Huang F, Rock JR, Harfe BD, Cheng T, Huang X, Jan YN, et al. Studies on expression and function of the TMEM16A calcium-activated chloride channel. Proc Natl Acad Sci U S A 2009;106:21413–8.
12. Hwang SJ, Blair PJ, Britton FC, O'Driscoll KE, Hennig G, Bayguinov YR, et al. Expression of anoctamin 1/TMEM16A by interstitial cells of Cajal is fundamental for slow wave activity in gastrointestinal muscles. J Physiol 2009;587:4887–904.
13. Gomez-Pinilla PJ, Gibbons SJ, Bardsley MR, Lorincz A, Pozo MJ, Pasricha PJ, et al. Ano1 is a selective marker of interstitial cells of Cajal in the human and mouse gastrointestinal tract. Am J Physiol Gastrointest Liver Physiol 2009;296:G1370–81.
14. Romanenko VG, Catalan MA, Brown DA, Putzier I, Hartzell HC, Marmorstein AD, et al. Tmem16A encodes the Ca^{2+}-activated Cl^- channel in mouse submandibular salivary gland acinar cells. J Biol Chem 2010;285:12990–3001.
15. Almaca J, Tian Y, Aldehni F, Ousingsawat J, Kongsuphol P, Rock JR, et al. TMEM16 proteins produce volume-regulated chloride currents

that are reduced in mice lacking TMEM16A. J Biol Chem 2009;284: 28571–8.
16. Elble RC, Pauli BU. Tumor suppression by a proapoptotic calcium-activated chloride channel in mammary epithelium. J Biol Chem 2001;276:40510–7.
17. Spitzner M, Martins JR, Soria RB, Ousingsawat J, Scheidt K, Schreiber R, et al. Eag1 and Bestrophin 1 are up-regulated in fast-growing colonic cancer cells. J Biol Chem 2008;283:7421–8.
18. Carles A, Millon R, Cromer A, Ganguli G, Lemaire F, Young J, et al. Head and neck squamous cell carcinoma transcriptome analysis by comprehensive validated differential display. Oncogene 2006;25: 1821–31.
19. Espinosa I, Lee CH, Kim MK, Rouse BT, Subramanian S, Montgomery K, et al. A novel monoclonal antibody against DOG1 is a sensitive and specific marker for gastrointestinal stromal tumors. Am J Surg Pathol 2008;32:210–8.
20. Kashyap MK, Marimuthu A, Kishore CJ, Peri S, Keerthikumar S, Prasad TS, et al. Genomewide mRNA profiling of esophageal squamous cell carcinoma for identification of cancer biomarkers. Cancer Biol Ther 2009;8:36–46.
21. Dagda RK, Zhu J, Kulich SM, Chu CT. Mitochondrially localized ERK2 regulates mitophagy and autophagic cell stress: implications for Parkinson's disease. Autophagy 2008;4:770–82.
22. Sun F, Mi Z, Condliffe SB, Bertrand CA, Gong X, Lu X, et al. Chaperone displacement from mutant cystic fibrosis transmembrane conductance regulator restores its function in human airway epithelia. FASEB J 2008;22:3255–63.
23. Silvis MR, Bertrand CA, Ameen N, Golin-Bisello F, Butterworth MB, Frizzell RA, et al. Rab11b regulates the apical recycling of the cystic fibrosis transmembrane conductance regulator in polarized intestinal epithelial cells. Mol Biol Cell 2009;20:2337–50.
24. Koppikar P, Lui VW, Man D, Xi S, Chai RL, Nelson E, et al. Constitutive activation of signal transducer and activator of transcription 5 contributes to tumor growth, epithelial-mesenchymal transition, and resistance to epidermal growth factor receptor targeting. Clin Cancer Res 2008;14:7682–90.
25. Fukazawa H, Mizuno S, Uehara Y. A microplate assay for quantitation of anchorage-independent growth of transformed cells. Anal Biochem 1995;228:83–90.
26. Reshmi SC, Huang X, Schoppy DW, Black RC, Saunders WS, Smith DI, et al. Relationship between FRA11F and 11q13 gene amplification in oral cancer. Genes Chromosomes Cancer 2007;46:143–54.
27. Ousingsawat J, Martins JR, Schreiber R, Rock JR, Harfe BD, Kunzelmann K. Loss of TMEM16A causes a defect in epithelial Ca^{2+}-dependent chloride transport. J Biol Chem 2009;284:28698–703.
28. MacLaine NJ, Wood MD, Holder JC, Rees RW, Southgate J. Sensitivity of normal, paramalignant, and malignant human urothelial cells to inhibitors of the epidermal growth factor receptor signaling pathway. Mol Cancer Res 2008;6:53–63.
29. Rathcke IO, Gottschlich S, Gorogh T, Lippert BM, Werner JA. [Incidence of point mutations in Ki-ras codon 12 and 13 in squamous epithelial carcinomas of the head-neck region]. Laryngorhinootologie 1996;75:465–70.
30. Stransky N, Egloff AM, Tward AD, Kostic AD, Cibulskis K, Sivachenko A, et al. The mutational landscape of head and neck squamous cell carcinoma. Science 2011;333:1157–60.
31. Agrawal N, Frederick MJ, Pickering CR, Bettegowda C, Chang K, Li RJ, et al. Exome sequencing of head and neck squamous cell carcinoma reveals inactivating mutations in NOTCH1. Science 2011;333:1154–7.
32. Kunzelmann K, Kongsuphol P, Chootip K, Toledo C, Martins JR, Almaca J, et al. Role of the Ca^{2+}-activated Cl^- channels bestrophin and anoctamin in epithelial cells. Biol Chem 2011;392: 125–34.
33. Namkung W, Phuan PW, Verkman AS. TMEM16A inhibitors reveal TMEM16A as a minor component of CaCC conductance in airway and intestinal epithelial cells. J Biol Chem 2011;286:2365–74.
34. Namkung W, Thiagarajah JR, Phuan PW, Verkman AS. Inhibition of Ca^{2+}-activated Cl^- channels by gallotannins as a possible molecular basis for health benefits of red wine and green tea. FASEB J 2010;24:4178–86.
35. Habela CW, Ernest NJ, Swindall AF, Sontheimer H. Chloride accumulation drives volume dynamics underlying cell proliferation and migration. J Neurophysiol 2009;101:750–7.
36. Habela CW, Olsen ML, Sontheimer H. ClC3 is a critical regulator of the cell cycle in normal and malignant glial cells. J Neurosci 2008;28: 9205–17.
37. Sontheimer H. An unexpected role for ion channels in brain tumor metastasis. Exp Biol Med (Maywood) 2008;233:779–91.
38. Galietta LJ. The TMEM16 protein family: a new class of chloride channels? Biophys J 2009;97:3047–53.
39. Hartzell HC, Yu K, Xiao Q, Chien LT, Qu Z. Anoctamin/TMEM16 family members are Ca^{2+}-activated Cl^- channels. J Physiol 2009;587: 2127–39.
40. Sheridan JT, Worthington EN, Yu K, Gabriel SE, Hartzell HC, Tarran R. Characterization of the oligomeric structure of the Ca^{2+}-activated Cl^- channel Ano1/TMEM16A. J Biol Chem 2011;286:1381–8.
41. Fallah G, Roemer T, Detro-Dassen S, Braam U, Markwardt F, Schmalzing G. TMEM16A(a)/anoctamin-1 shares a homodimeric architecture with CLC chloride channels. Mol Cell Proteomics 2011;10: M110.004697.
42. Carneiro A, Isinger A, Karlsson A, Johansson J, Jonsson G, Bendahl PO, et al. Prognostic impact of array-based genomic profiles in esophageal squamous cell cancer. BMC Cancer 2008;8:98.
43. West RB, Corless CL, Chen X, Rubin BP, Subramanian S, Montgomery K, et al. The novel marker, DOG1, is expressed ubiquitously in gastrointestinal stromal tumors irrespective of KIT or PDGFRA mutation status. Am J Pathol 2004;165:107–13.
44. Ayoub C, Wasylyk C, Li Y, Thomas E, Marisa L, Robe A, et al. ANO1 amplification and expression in HNSCC with a high propensity for future distant metastasis and its functions in HNSCC cell lines. Br J Cancer 2010;103:715–26.
45. Tian Y, Kongsuphol P, Hug M, Ousingsawat J, Witzgall R, Schreiber R, et al. Calmodulin-dependent activation of the epithelial calcium-dependent chloride channel TMEM16A. FASEB J 2011; 25:1058–68.
46. Ferrera L, Caputo A, Ubby I, Bussani E, Zegarra-Moran O, Ravazzolo R, et al. Regulation of TMEM16A chloride channel properties by alternative splicing. J Biol Chem 2009;284:33360–8.
47. Ferrera L, Scudieri P, Sondo E, Caputo A, Caci E, Zegarra-Moran O, et al. A minimal isoform of the TMEM16A protein associated with chloride channel activity. Biochim Biophys Acta 2011;1808: 2214–23.
48. Mazzone A, Bernard CE, Strege PR, Beyder A, Galietta LJ, Pasricha PJ, et al. Altered expression of Ano1 variants in human diabetic gastroparesis. J Biol Chem 2011;286:13393–403.